# Unique Molecular Dynamics of Structural Elements in an Asymmetric Janus Bisamide Supramolecule Characterized by Solid-State NMR

Wei Chen,[†] Hao-Jan Sun,[‡] and Toshikazu Miyoshi*,[†]

[†]Department of Polymer Science, The University of Akron, Akron, Ohio 44325-3909, United States

[‡]Roy & Diana Vagelos Laboratories, Department of Chemistry, University of Pennsylvania, Philadelphia, Pennsylvania 19104-6323, United States

Ⓢ *Supporting Information*

ABSTRACT: An asymmetric tapered Janus bisamide supramolecule consisting of 1,4-bis[3,4,5-tris(alkan-1-yloxy)benzamido]benzene bisamide (abbreviated as $C_{22}PhBAEO_3$) can possess three-dimensional (3D) long-range order under mild thermal treatment conditions. To understand its structural formation and unique phase-transition processes, the locally detailed structure and molecular dynamics of its structural elements in disordered and ordered phases of $C_{22}PhBAEO_3$ were investigated using various solid-state (SS) NMR techniques at the atomic level. On the basis of the determined conformations and packing structures of the alkyl chains in ordered and disordered crystalline phases, along with the geometry and kinetic parameters of the structural elements' dynamics, this study addresses the self-assembly, the phase-transition mechanisms, and the relationship between the structure and dynamics of these asymmetric Janus bisamide supramolecules.
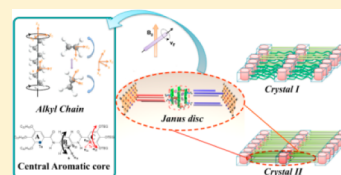
1. INTRODUCTION

Self-assembled supramolecules consist of molecules with different structural elements that typically include rigid and flexible parts. Molecules interact with each other via secondary interactions such as $\pi-\pi$ interactions, hydrogen bonding, electrostatic interactions, van der Waals interactions, and rigid/flexible and hydrophobic/hydrophilic repulsions.[1−3] Complex supramolecules can commonly be divided into several common classifications, such as spheres, cylinders, or discs, on the basis of their dimensions and architectures. In many cases, however, self-assembly systems include more or less structural disorder in their flexible parts, which significantly influences their functional properties.[4,5] Consequently, structural control of these flexible parts is one of the most important issues in supramolecular science. Investigations of the structure and dynamics of complex supramolecules at various length and time scales are essential to understanding their self-assembly mechanisms and improving their functions.[6,7]

A recently synthesized asymmetric tapered Janus bisamide compound, 1,4-bis[3,4,5-tris(alkan-1-yloxy)benzamido]-benzene bisamide (abbreviated as $C_{22}PhBAEO_3$), consists of a rigid core with three aromatic rings in the middle, hydrophilic methyl-terminated ethylene glycol tails with three repeat units (triethylene glycol, or TEG) at one end, and hydrophobic alkyl chain tails with 22 carbon numbers at the other end, as illustrated in Scheme 1.[8] A combination of wide-angle X-ray diffraction (WAXD), small-angle X-ray scattering (SAXS), electron diffraction (ED), and computer simulations indicates that $C_{22}PhBAEO_3$ can form three unique versions—"crystal I", "crystal II", and "columnar phases"—depending on its thermal history (Figure 1a), and only the crystal II phase possesses 3D long-range order ($a = 5.08$, $b = 2.41$, $c = 0.98$ nm, $\alpha = \beta = 90°$, and $\gamma = 70.5°$). A structural formation process for the 3D long-

range order is also suggested. In the first process, four molecules make one disc via intermolecular hydrogen bonding between N−H and C=O groups in the central aromatic cores, as illustrated in Figure 1b), where two molecules are orthogonal to each other through intermolecular hydrogen bonding. Four molecules compose one disc. The second process is the formation of the asymmetric ellipsoid cylinder as a result of disc stacking. All discs interact with each other via the same hydrogen-bonding interactions used in the first-level structure, as illustrated in Figure 1c. Actually, the columnar phase can be formed when the melts are cooled to less than 358 K, and this phase possesses regularly stacked central cores with a d-spacing of 0.7−1.0 nm. The long d-spacing is a characteristic structure for the hydrogen-bonding columnar phase, which is much longer than the sheet-type aromatic core structures with a d-spacing of 0.35 nm, such as triphenylene[9] and hexa-*peri*-hexabenzocoronene (HBC) derivatives.[10] The literature contains numerous reports of molecular dynamic investigations on traditional columnar systems because the molecular dynamics of aromatic cores significantly influence the charge-carrier mobility in photovoltaic devices.[10−12] However, few investigations into the molecular dynamics of the newly designed hydrogen-bonded aromatic core have been published. In addition, two aromatic rings at either end of the core are also chemically connected to two different flexible chains, including hydrophobic alkyl and hydrophilic TEG chains, via flexible −O− linkages. Thus, not only the spacing but also the mobility and phase structures of the hydrophobic/hydrophilic chains are expected to significantly influence the dynamics of these two
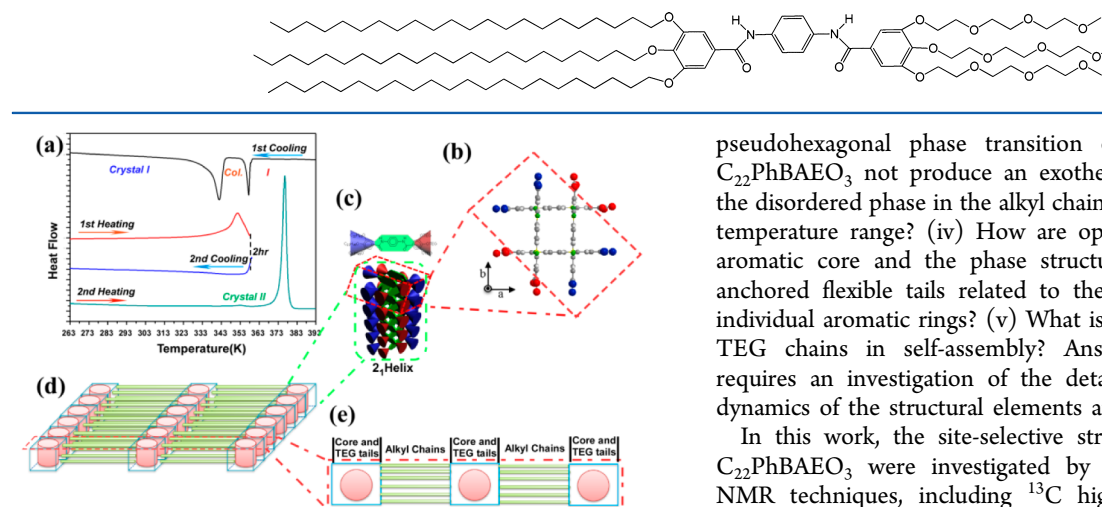
Scheme 1. Chemical Structure of $C_{22}PhBAEO_3$

Figure 1. (a) DSC thermal diagram of C22PhBAEO₃ at a scan rate of 10 K/min. The sample was cooled directly from its isotropic melt state and then heated to 360 K and annealed for 2 h. The bottom two diagrams show the subsequent cooling and heating processes. (b) The basic orthogonal Janus disc view from crystallographic $a-b$ plane.[8] The red and blue balls represent hydrophilic triethylene glycol (TEG) and hydrophobic aliphatic chains, respectively. (c) The 2_1 helical packing of the basic Janus disc. (d) The 3D schematic illustration and (e) top view of the Janus disc packing structure (crystal II).

aromatic rings. The third-level structure consists of the packing of individual cylinders via hydrophobic and hydrophilic repulsion, which induces phase separations between the two types of flexible chains (Figure 1d, e). This process includes crystallization of the alkyl chains. Cooling of the columnar phase kinetically induces formation of the metastable crystal I phase, which does not have a long-range order in the alkyl chains. However, the detailed static and dynamic structures are not yet understood. In addition, the annealing of the crystal I phase cannot lead to the thermodynamically stable crystal II phase, which is formed only via annealing of the columnar phase. Only one process can achieve 3D long-range order in $C_{22}PhBAEO_3$, where the alkyl chains have long-range order in the orthorhombic phase and the hydrophilic TEG chains lack long-range order.[8]

Moreover, WAXD indicated that the alkyl chains in the crystal II phase possess unique structural features, such as phase transitions from orthorhombic to pseudohexagonal above 323 K, which do not accompany the exothermic peak in the heating process, and a very high melting temperature of the pseudohexagonal phase (377 K).[8] These unique features of the alkyl chains differ substantially from the thermal behaviors of n-alkanes, which commonly exhibit phase transitions from triclinic (odd number) and orthorhombic (even number) to hexagonal.[13−16] All phase transitions accompany the exothermic peak during individual transition processes. In addition, the hexagonal phase exhibits a melting temperature (303−343 K) that is much lower than that of the alkyl chains in $C_{22}PhBAEO_3$.[16] The observed thermal behaviors of the alkyl chains in $C_{22}PhBAEO_3$ are intrinsic properties in its self-assembly.

The following questions arise concerning $C_{22}PhBAEO_3$: (i) Why can the crystal II phase only be formed with the columnar phase as a precursor? (ii) Why does the orthorhombic to

pseudohexagonal phase transition of the alkyl chains in $C_{22}PhBAEO_3$ not produce an exothermic peak? (iii) Why is the disordered phase in the alkyl chains maintained over a wide temperature range? (iv) How are open spaces in the central aromatic core and the phase structure and mobility of the anchored flexible tails related to the molecular dynamics of individual aromatic rings? (v) What is the role of hydrophobic TEG chains in self-assembly? Answering these questions requires an investigation of the detailed local structure and dynamics of the structural elements at the atomic level.

In this work, the site-selective structure and dynamics of $C_{22}PhBAEO_3$ were investigated by various solid-state (SS) NMR techniques, including ^{13}C high-resolution NMR and comparisons of relaxation times, in addition to studies of the anisotropic interactions (i.e., chemical-shift anisotropy (CSA) and dipole−dipole interactions). First, the conformation and molecular dynamics of the alkyl chains in the crystal I and II phases as functions of temperature were investigated using high-resolution NMR, CSA, and dipolar interactions. These investigations illustrated the differences and similarities between detailed conformations and the molecular dynamics of the alkyl chains between the crystal I and II phases. Second, the molecular dynamics of TEG chains were also investigated. Finally, the characteristic dynamics of three aromatic rings influenced by the space produced by unique hydrogen bonding, phase structures, and mobility of chemically anchored flexible chains were studied. Several answers to the previously stated questions are given based on the obtained experimental and simulated results.

2. EXPERIMENTAL SECTION

2.1. Sample. The synthetic route and detailed characterization results of $C_{22}PhBAEO_3$ can be found in the corresponding literature.[8] We obtained the crystal I phase directly by cooling the sample from the melted state at 10 K/min after the sample was annealed at 393 K for 10 min. We obtained the most stable phase, crystal II, by annealing the columnar phase for 2 h at 360 K (Figure 1a).

2.2. Solid-State NMR Measurements. The NMR experiments were performed on a Bruker Avance 300 with carrier frequencies of 300.3 and 75.5 MHz for ^{1}H and ^{13}C, respectively. All experiments were performed using a 4 mm double-resonance probe. The chemical shift was externally referred to the methine peak of adamantine at 29.46 ppm, and the temperature inside the sample was calibrated using the [207]Pb chemical shift of Pb(NO₃)₂.[17] The rf field strength for both ^{1}H and ^{13}C was fixed at 62.5 kHz, whereas the [1]H−[13]C cross-polarization (CP) time and recycle delay (RD) time were 2 ms and 2 s, respectively. The MAS spinning frequency was set to 6 kHz. [1]H two-phase pulse modulation (TPPM) with a field strength of 62.5 kHz was applied during the ^{13}C signal acquisition. The RD time was set to 6 s in the direct polarization (DP) MAS experiment.

2.2.1. 2D [1]H−[13]C WISE.[18] The [1]H 90° pulse was set to 4 μs, and a CP contact time of 100 μs was used to minimize the ^{1}H spin-diffusion effect. The total sideband suppression (TOSS)[19] sequence was used to suppress spinning sidebands during signal

detection.[18] Spectral widths in the ω_1 and ω_2 dimensions were set to 200 and 25 kHz, respectively. The ^{1}H wide-line separation (WISE) NMR experiments were performed using time-proportional phase incrimination (TPPI)[20] in the t_1 dimension with 256 scans. The other parameters were the same as those used for CP/MAS.

2.2.2. 2D SUPER.[21] Separation of undistorted powder patterns by effortless recoupling (SUPER) is used to get CSA information. These experiments were performed at MAS frequencies of 3 kHz for the alkyl chain and TEG tails and 5 kHz for the aromatic carbons. The scaling factor, χ', was 0.155 in our experiment. Thus, the effective spectral widths in indirect dimension were 3 kHz/0.155 = 19 kHz and 5 kHz/0.155 = 32 kHz for the alkyl chain and aromatic core, respectively. For the required ^{13}C 2π pulse strength, ω_C, and angular frequency, ω_r, $\omega_C = 12.12 \times \omega_r$, and the corresponding pulse strengths were set to 36 and 61 kHz. A ^{1}H continuous wave (CW) decoupling with a field strength of 100 kHz was applied during CSA recoupling. The numbers of t_1 increments for the alkyl and aromatic carbons were 64 and 32, respectively, and TOSS[19] was used during the ^{13}C signal acquisition process. The states-TPPI was set to acquisition mode.

2.2.3. ^{1}H–^{13}C DIPSHIFT..[22-25] The CP contact time was set to 600 μs, and the frequency-switched Lee–Goldburg (FSLG)[26] was used during the evolution period to decouple proton homonuclear interaction with a duration of 18.14 μs per 2π pulse. The MAS frequency was set to 7 kHz, and the data were acquired at every $t_r/8$ period along the t_1 domain.

2.3. NMR Theory. *2.3.1. Magnetic Anisotropic Interactions.* In solids, nuclear magnetic anisotropic interactions such as CSA and dipole–dipole interactions exhibit an angular orientation relative to the external magnetic field. The resonance frequency of the magnetic anisotropic interactions can be written as[27]

$$\omega(\theta, \varphi) = \frac{1}{2}\delta[3\cos^2\theta - 1 + \eta\sin^2\theta\cos^2(2\varphi)] \tag{1}$$

where (θ,φ) is the polar angle of the external magnetic field $\vec{B_0}$ in the principal axis system (PAS) of the interaction tensor, and η and δ are the asymmetry and anisotropy parameters, respectively. When the molecules undergo dynamics in a fast limit motion ($\tau_c\delta \gg 1$, where τ_c is the correlation time), the averaged frequency $\bar{\omega}$ is described in terms of[27,28]

$$\bar{\omega}(\Theta, \Psi) = \frac{1}{2}\bar{\delta}[3\cos^2\Theta - 1 + \bar{\eta}\sin^2\Theta\cos(2\Psi)] \tag{2}$$

where (Θ,Ψ) are the polar coordinates of the external magnetic field $\vec{B_0}$ in the averaged principle axes system (PAS) of the averaged tensor, and $\bar{\delta}$ and $\bar{\eta}$ are the averaged anisotropy and averaged asymmetry parameters, respectively.

The averaged interaction tensor $\bar{\sigma}$ in the available site numbers of N can be written as

$$\bar{\sigma} = \sum_{i=1}^{N} p_i\sigma_i \tag{3}$$

where p_i represents the probability for each site, and σ_i is the interaction tensor at each site.

2.3.2. DIPSHIFT. The dipolar-chemical shift correlation (DIPSHIFT) selectively retains the heteronuclear dipolar coupling interaction as the only interaction factor during a spin evolution time, t_1, that ranges from 0 to one rotor period,

t_r, of MAS. The DIPSHIFT curves for CH and CH$_2$ as functions of the evolution time t_1 can be represented as[22-24]

$$\text{CH:} \quad \frac{I(t_1)}{I_0} = \langle\cos\Phi\rangle_{\alpha,\beta,\gamma}$$

$$\text{CH}_2: \quad \frac{I(t_1)}{I_0} = \frac{1}{2}\langle\cos(\Phi_1 - \Phi_2)\rangle_{\alpha\beta\gamma}$$
$$+ \frac{1}{2}\langle\cos(\Phi_1 + \Phi_2)\rangle_{\alpha\beta\gamma} \tag{4}$$

where the angle brackets represent the powder average over the Euler angle of (α,β,γ), and Φ is the phase of the magnetization acquired by the ^{1}H–^{13}C dipolar interactions within an evolution time t_1

$$\Phi = \int_{t_1}^{0} D_{ZZ}^{LF}(t)\,\mathrm{d}t$$

where $D_{ZZ}^{LF}(t)$ is the ZZ component of the dipolar tensor in the laboratory frame. The CH$_2$ case accounts for two CH dipolar interactions; thus, Φ_1 and Φ_2 in eq 4 are the phases of the magnetization acquired under the interactions for two different protons of the CH$_2$ group. Therefore, the DIPSHIFT curves include dipolar coupling strengths modulated by molecular dynamics.[22,25]

2.3.3. ^{13}C Line Width (T_2) under ^{1}H Decoupling. Molecular dynamics can also be obtained on the basis of the ^{13}C line width that is related to the spin–spin relaxation time T_2. The ^{13}C line width under high-power decoupling can be expressed as[29]

$$\kappa = (\pi T_{20})^{-1} + (\pi T_{2c})^{-1} + (\pi T_{2m})^{-1} \tag{5}$$

where $(\pi T_{20})^{-1}$ represents the intrinsic line width due to external factors such as the homogeneity of the static field, $(\pi T_{2c})^{-1}$ shows the distribution of the isotropic chemical shift, and $(\pi T_{2m})^{-1}$ accounts for factors caused by segmental motion.[29,30] Two mechanisms have been proposed to explain the third term.[29-32] One mechanism is the interference between molecular motions and ^{1}H dipolar decoupling. The other mechanism is the modulation of CSA caused by molecular motion with that caused by MAS. Therefore, when the motional frequency reaches the decoupling or MAS frequency, a maximum motional broadening is observed.

The empirical expression for the second term is[29]

$$(\pi T_{2c})^{-1} = \kappa_I\left[1 + \frac{2}{\pi}\arctan(\alpha(T_0 - T))\right] \tag{6}$$

where κ_I is the full width of the carbon resonance line at half-height due to the distribution of an isotropic chemical shift, α reflects the steepness of this narrowing ($0 \leq \alpha \leq 1$), and T_0 is the onset transition temperature.

When dipolar coupling strength is the dominant factor, the third term is

$$(\pi T_{2m})^{-1} = \lambda M_2 J(\omega_1, \tau) \tag{7}$$

and additionally

$$M_2 = \frac{\gamma_H^2\gamma_C^2 h^2}{5r^6}, \quad J(\omega_1, \tau) = \frac{\tau}{1 + \tau^2\omega_1^2}$$

where γ_C and γ_H are gyromagnetic ratios of carbon and proton, respectively, h is the plank constant, r is the C–H internucleus distance, ω_1 is the decoupling strength, and λ is a scaling factor

$(0 \leq \lambda \leq 1)$. In our research, we assumed that the correlation time simply followed an Arrhenius-type temperature dependence, $\tau_c = \tau_0 e^{(E_a/(RT))}$.

3. RESULTS

3.1. ^{13}C CP/MAS Spectra.
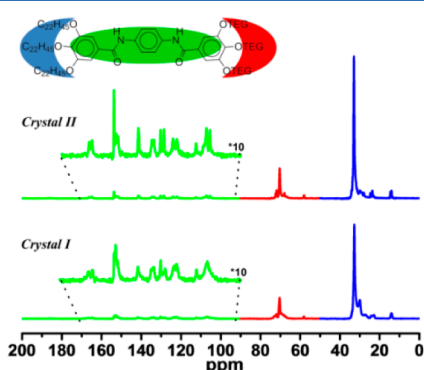Figure 2 shows the ^{13}C CP/MAS spectra of the crystal I and II phases at 333 K. Three

Figure 2. ^{13}C CP/MAS NMR spectra of Janus bisamide within the crystal I and II phases, together with a vertically enlarged picture of the central aromatic carbons at 333 K.

different functional groups of the aromatic core, aliphatic, and TEG regions are clearly separated from each other and are displayed in different colors. These well-separated signals provided us with the opportunity to extract site-specific structures and dynamics using various NMR techniques. The following sections describe the molecular structure and dynamics of these three parts in succession.

3.2. Conformation and Packing of the Alkyl Chains.
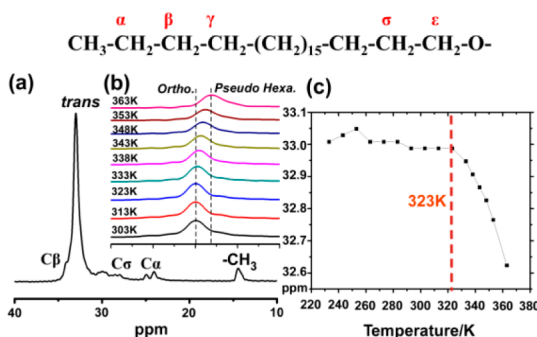Figures 3a illustrates the ^{13}C CP/MAS NMR spectra of the

Figure 3. (a) ^{13}C CP/MAS NMR spectrum of the aliphatic regions in the crystal II phase at ambient temperature along with the signal assignments. (b) Temperature dependence of the inner alkyl carbons' ^{13}C CP/MAS NMR spectra and (c) the corresponding chemical shifts.

alkyl chains in the crystal II phase at ambient temperature. The peaks were assigned on the basis of previous results about macromolecules with alkyl chains[33] and n-alkanes.[34,35] The ^{13}C chemical shift of the alkyl chains is very sensitive to both conformations and packing structures.[27,33−35] With respect to the crystal II phase, the chemical shift of the inner alkyl chains (33 ppm) is consistent with the reported values for n-alkanes and PE in the crystalline regions, which adopt the *trans* conformation; its conformation was therefore assigned as *trans*.[27,33−35]

Figure 3, b and c, shows the temperature dependencies of the ^{13}C CP/MAS NMR spectra for the inner carbons of the alkyl chains in the crystal II phase and the corresponding chemical shifts, respectively. The resonance line at 33.0 ppm gradually moved to the upfield side at temperatures greater than 323 K and finally reached 32.6 ppm at 363 K. This upfield shift was attributed to the phase transition from orthorhombic to pseudohexagonal.[8]

n-Alkanes with carbon numbers between 11 and 40,[13−15] ultradrawn polyethylene (PE) under ambient pressure,[36,37] and PE under high pressure[38] are well-known to undergo phase transitions from their crystalline states to their hexagonal phases. For example, Ishikawa et al. have reported an approximately 0.5 ppm downfield ^{13}C chemical shift of n-$C_{19}H_{40}$ during its phase transition from 288 to 308 K.[35] The observed downfield shift was attributed to a packing effect[39] because n-alkanes retain all-*trans* zigzag conformations during this phase transition, as confirmed by X-ray diffraction[40] and Raman spectroscopy.[41] However, the ^{13}C chemical shift of PE moved to the upfield side during its orthorhombic/hexagonal transition. This upfield shift was attributed to the increasing *gauche* conformation and rapid transition between *trans* and *gauche*, together with the packing effect.[42] When one carbon adopts a *gauche* conformation with respect to carbon in the γ-position, the ^{13}C chemical shift moves to the upfield side by approximately 5 ppm with respect to the chemical shift exhibited by a carbon in a *trans* conformation. This empirical rule is called the γ-*gauche* effect.[35] In chemical shift analyses of both n-alkanes (odd) and PE, the packing change was assumed to induce a small downfield shift of approximately 0.5 ppm. Thus, the two competing effects of packing and conformation were thought to lead to the apparent upfield shift of the alkyl chains' ^{13}C signal in the crystal II phase. The observed upfield shift of the alkyl chains was empirically interpreted in terms of the ^{13}C chemical shift difference between the two phases (0.5 ppm), the γ-*gauche* effect,[27,43] and a fraction of the *gauche* conformation, f_g, as follows[42]

$$-2 \times 5.0 \times f_g + 0.5 = 32.6 - 33.0 \qquad (8)$$

where the coefficient of 2 in the first term represents two carbons in γ-positions.[35,39,44] Using eq 8 and the observed chemical shift, f_g was estimated to be 9% at 363 K.

Figure 4a shows the ^{13}C CP/MAS spectrum of the alkyl chain in the crystal I phase, where two signals for the inner alkyl chain are observed at 33.0 and 30.0 ppm. The former was assigned to the *trans* conformation in the crystalline region. As previously mentioned, the ^{13}C chemical shift can distinguish the
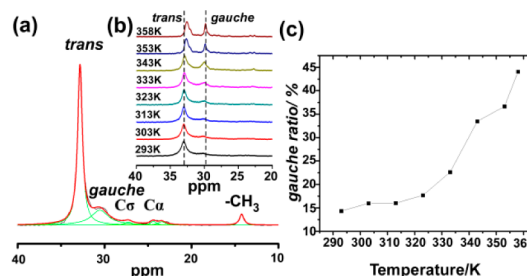

Figure 4. (a) ^{13}C CP/MAS NMR of the aliphatic carbon in the crystal I phase. (b) ^{13}C DP/MAS NMR spectra of the inner alkyl carbon in the crystal I phase and (c) the fraction of the *gauche*-rich component (simplified as *gauche* in the Figure) as a function of temperature.
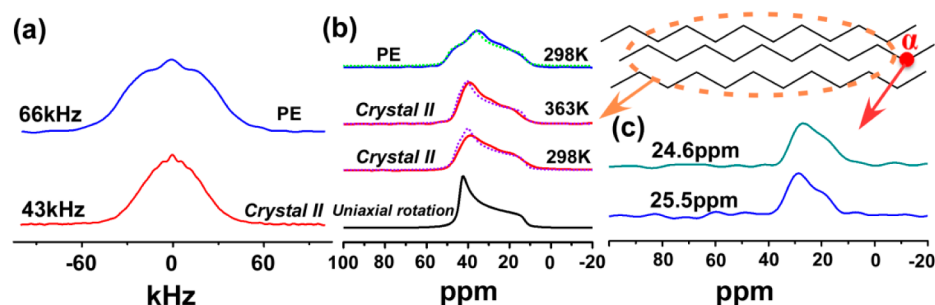
Figure 5. (a) ^{1}H slice data for WISE spectra of the inner alkyl chains in the crystal II phase (blue) and the crystalline component of polyethylene (PE) (red) at ambient temperature; ^{13}C experimental (solid curve) and simulated (dotted) CSA spectra of (b) the inner alkyl chains in the crystal II phase and the crystalline PE and (c) the terminal α-group.

orthorhombic from the triclinic phase; i.e., the observed chemical shift was assigned to the signals of the *trans* conformation in the orthorhombic phase, which was the same structure as that of the crystal II phase. The latter signal appeared at 30.0 ppm, corresponding to a highly disordered conformation (or *gauche*-rich conformation). Two conformations were included in the crystal I phase.

The CP step modulated the ^{13}C signal intensities depending on the ^{13}C–^{1}H dipolar coupling strength and the spin−lattice relaxation time in the rotating frame ($T_{1\rho}$). To quantitatively analyze fractions of the two conformations, we applied ^{13}C DP at a recycle delay of 6.0 s, which was set to 5 times the longest T_1 value for the alkyl chains (1.1 s) at ambient temperature. Notably, the T_1 values of the inner alkyl chains in $C_{22}PhBAEO_3$ are much shorter than the reported T_1 values of *n*-alkane (e.g., *n*-$C_{27}H_{56}$, 160 s)[34] and PE crystalline regions (2000 s) at ambient temperature.[36] The short T_1 value indicates a very high mobility of the alkyl chains, even in the crystalline state. A detailed discussion of molecular dynamics is given later. Figure 4b shows the ^{13}C DP/MAS NMR spectra of the alkyl chains in the crystal I phase at various temperatures. Two spectral changes were observed with increasing temperature. One change was an upfield shift of the inner alkyl chains from 33.0 ppm at ambient temperature to 32.6 ppm at 358 K. This upfield shift was almost the same as that of the alkyl chain in the crystal II phase, which implies that the ordered alkyl chains in the crystal I phase experienced the same phase transition as those in the crystal II phase. Specifically, the orthorhombic/pseudohexagonal transition occurred in the ordered alkyl chains in both the crystal I and crystal II phases.

Another interesting feature was the increasing fraction of the *gauche*-rich conformation at 30.0 ppm with increasing temperatures. The ^{13}C chemical shift of the *gauche*-rich signal was almost invariant up to 358 K, which was slightly higher than the melting temperature of the crystal I phase (351 K). Thus, the highly disordered conformation at ambient temperature was almost the same as the conformations in the melted state. Using eq 8 and the observed chemical shift value, we estimated the fraction of the *gauche*-rich conformation at various temperatures; the results are illustrated in Figure 4c. The fraction of the *gauche*-rich conformation clearly increased from 14% at ambient temperature to 44% at 358 K. This NMR result clearly indicates that local melting of the alkyl chain originated from the crystal I/columnar phase transition. A similar result has been observed in the phase transition of the alkyl chains in symmetric bisamide.[45,46] Notably, the complete melting of the alkyl chains in the crystal I phase was not observed in our experiment because the phase transition from the columnar

phase to the crystal II phase occurred simultaneously at the same temperature. Two different processes contributed to the apparent *trans*-rich conformation at 32.6 ppm, even at temperatures above the crystal I/columnar phase-transition temperature.

High-resolution NMR clearly indicated that two different conformations were included in the crystal I phase. At least two different possible structures could explain the results observed for the crystal I phase. In one case, individual alkyl chains may locally adopt structural disorders, including the ordered and melted regions. For example, the interior and chain ends may adopt ordered and melted states, respectively. The other case is a spatial distribution of two structures over entire samples. In this case, some molecules may adopt ordered structures, whereas the remaining molecules may possess disordered structures. The latter case would likely create domain structures at certain lengths. Intermediate structures between the two could also be possible. A clarification of the structure is given in a later section.

A comparison of the ^{13}C high-resolution NMR spectra for the crystal I and crystal II phases indicated a unique structure for the alkyl chains at the chain ends. In the crystal I phase, the $C\alpha$ carbon signal was split into doublet and asymmetric line shapes (Figure 4a), whereas the crystal II phase gave an unresolved but asymmetric line shape. The observed doublet line and asymmetric shapes provided different magnetic environments for the chain ends within the crystal I and II phases. The well-resolved signals clearly gave two different environments for the terminal chains in the crystal II phase, but broad signals indicated continuous disorder in the crystal I phase. Therefore, the $C\alpha$ signals were used for a site-selective dynamic investigation via recoupled CSA.

3.3. Molecular Motions of the Alkyl Chains. WISE NMR is a direct method that can correlate molecular mobility along the ^{1}H dimension in structures using highly resolved ^{13}C signals.[18,28,33] In organic molecules, the ^{1}H full line width at half-height (flwhh) is typically ca. 50−60 kHz in a rigid limit, depending on the ^{1}H density. If the motional frequency exceeds the static line width, the ^{1}H line width decreases depending on the dynamic geometry. Figure 5a shows ^{1}H slice data for the inner alkyl carbon in the crystal II phase and, for comparison, for linear low-density PE (LLDPE) at 298 K. The alkyl chains in the crystal II phase had a ^{1}H line width of 43 kHz at flwhh, which was much narrower than that of the crystalline component of LLDPE (ca. 66 kHz). The observed narrowed ^{1}H line width indicated molecular dynamics even in the crystalline phase (crystal II) at a fast motional limit (>60 kHz). This result is consistent with the short ^{13}C T_1 value of 1.1 s.
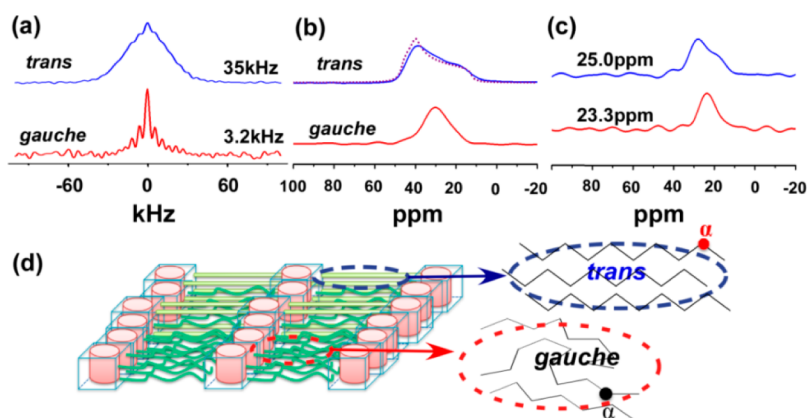
Figure 6. (a) ^{1}H WISE slice data of the alkyl chain's inner carbons in the crystal I phase with *trans*-rich (blue) and *gauche*-rich (red) regions at ambient temperature; (b) experimental and simulated (dotted purple) ^{13}C CSA spectra of the inner carbons with *trans*-rich (blue) and *gauche*-rich (red) in the crystal I phase, along with a simulated curve (dotted); and (c) ^{13}C CSA spectra of the terminal α-carbon obtained through ^{13}C high-resolution NMR signals at 23.3 (red) and 25.0 ppm (blue). (d) Schematic illustration of crystal I structure. Cylinder parts representing the bisamide and TEG chains, and straight and curved green lines illustrating the alkyl chains in *trans* (ordered) and *gauche*-rich (melt state) conformations, respectively.

Very fast motions effectively average out the ^{13}C CSA of the alkyl chains. Thus, the geometry of molecular motions of the alkyl chains was further investigated by the recoupled CSA. The second and third spectra from the top in Figure 5b illustrate the ^{13}C CSA spectra of the inner alkyl chains in the crystal II phase at ambient temperature (orthorhombic phase) and at 363 K (pseudohexagonal phase), respectively. For comparison, the ^{13}C CSA of the CH$_2$ group of LLDPE is also shown at the top of Figure 5b. The CSA spectrum of the LLDPE showed an asymmetric pattern with principal values of $(\sigma_{11}, \sigma_{22}, \sigma_{33}) = (50, 36.5, 12.5$ ppm$)$, which are consistent with the reported values.[21] However, the CSA of the CH$_2$ group for the inner alkyl chains in the crystal II phase showed an axially symmetric pattern with $(\sigma_{11}, \sigma_{22}, \sigma_{33}) = (46, 39, 14$ ppm$)$, which were almost the same as the principal values in the pseudohexagonal phase $((\sigma_{11}, \sigma_{22}, \sigma_{33}) = (45, 39.5, 13.5$ ppm$))$.

In PE and *n*-alkanes, the CSA principal axes adopt the following orientations: σ_{11} (50 ppm) is parallel to the H−H vector, σ_{22} (36.5 ppm) is parallel to the H−C−H bisector angle, and σ_{33} (12.5 ppm) is perpendicular to the H−C−H plane or parallel to the chain axis. In the current study, the molecular dynamics of the inner alkyl chains could not be frozen at a temperature of 233 K. The dynamic geometry was considered under the assumptions that the principal axis values and orientations of the ^{13}C shielding tensor in the inner alkyl chains of the crystal II phase and the same pseudohexagonal phase are the same as those of HDPE. The invariant σ_{33} value of the motionally averaged CSA indicated that the axis of the alkyl chains corresponded to the dynamic axis. The effect of the reorientation angle φ on the CSA patterns was calculated by assuming a two-site jump motion. On the basis of eqs 1−3, the eigenvalues of the motionally averaged tensor, $\overline{\sigma}$, $\overline{\eta}$, and $\overline{\delta}$ were calculated as

$$\overline{\sigma_{11,22}} = \frac{1}{2}[(\sigma_{11}^{\mathrm{PAS}} + \sigma_{22}^{\mathrm{PAS}}) \pm |\cos\varphi(\sigma_{11}^{\mathrm{PAS}} - \sigma_{22}^{\mathrm{PAS}})|],$$

$$\overline{\sigma}_{33} = \sigma_{33}^{\mathrm{PAS}} \tag{9}$$

and

$$\overline{\eta} = |\cos\varphi|\eta_0, \qquad \frac{\overline{\delta}}{\delta} = 1 \tag{10}$$

The reorientation angle dependencies of $\overline{\eta}$ and $(\overline{\delta})/(\delta)$ were estimated using eq 10 and are illustrated in Figure S1(b) in the Supporting Information. The $\overline{\eta}$ value was highly dependent on φ. When φ increased, the $\overline{\eta}$ value decreased and became 0 at $\varphi = 90°$. A further increase in φ increased the $\overline{\eta}$ value to its original value. The calculated spectrum with $\varphi = 60/120°$ and a Lorentzian broadening of 3 ppm (the second dotted spectrum from the top in Figure 5b) effectively reproduced the experimental CSA spectrum of the crystal II phase (the second solid spectrum). Even in the pseudohexagonal phase, a similar reorientation angle of 65° could reproduce the experimental data (the third spectrum from the top in Figure 5b). The uniaxially rotational diffusion of a rigid body was also calculated as a reference (bottom of Figure 5b). The calculated spectral pattern was substantially different from the experimental results for both phases. Thus, we concluded that the uniaxial diffusions observed in the PE and *n*-alkanes in the hexagonal phases were not present in the pseudohexagonal phase of the alkyl chains in the crystal II phase.

Figure 5c depicts the ^{13}C CSA obtained through the split peaks at 24.6 and 25.5 ppm of the terminal α-carbons in the crystal II phase (see Figure 3a). Both CSA spectra showed axially symmetric patterns, as observed in the inner alkyl chains. This result indicates that the chain ends at the two magnetically inequivalent sites had the same geometry as the inner carbons in both the orthorhombic and pseudohexagonal phases of the crystal II phase. Specifically, the entire alkyl chains homogeneously showed the same dynamic geometry from the inner part to the end of the crystal II phase.

Figure 6a shows the ^{1}H WISE slice spectra for the inner carbons in different conformations in the crystal I phase at ambient temperature. The line width of the *trans* conformation was 35 kHz, which is slightly narrower than that of the crystal II phase (43 kHz). This comparison suggests that the motional frequency in the crystal I phase is slightly higher than that in the crystal II phase. However, the *gauche*-rich conformation in the crystal I phase provided a very narrowed ^{1}H line width of 3.2 kHz, indicating that the alkyl chains in the *gauche*-rich conformation had nearly isotropic motion, even in the crystal I phase. In addition, the corresponding CSA spectra directly proved different dynamic geometries in two conformations of the alkyl chains in the crystal I phase (Figure 6b). The alkyl

chains in the *trans* conformation showed an axial symmetric pattern that was very similar to that in the crystal II phase (top of Figure 6b). The calculated spectrum with a best-fit φ value of 60° (dotted line in Figure 6b) accurately reproduced the experimental spectrum. The CSA line shape in the highly disordered conformation indicates a largely averaged line shape at the isotropic chemical shift, which indicates near-isotropic motions in the *gauche*-rich conformation; this near-isotropic motion differs substantially from that in the *trans* conformation.

Figure 6c shows the CSA pattern of the terminal α-carbons in the crystal I phase. The terminal α-carbons also produced two different CSA line shapes. The CSA spectrum at 25.0 ppm gave axial symmetric pattern very similar to that for the α-carbon in the crystal II phase, whereas that at 23.3 ppm showed a near-isotropic component. The two components observed at the terminal carbons were consistent with the results for the inner carbons. Both the inner and end parts of the alkyl chains possessed very different dynamic geometries in their uniaxial rotations and near-isotropic motions, which indicate that some regions consisting of multiple alkyl chains adopted locally ordered (all-*trans* conformation) and disordered structures in space. Previous WAXD results could not be used to identify 3D long-range order in the crystal I phase.[8] This fact suggests the ordered and disordered structures make small domains on the scale of a few nanometers or less. Schematic representations of the dynamic and structural models are also illustrated in Figure 6d. The site-selective observation of local molecular dynamics (anisotropic interaction) and structures (isotropic interaction) for the inner and end parts indicates that two independent structures of the ordered and melted states are separated from each other on a few nanometers or less in the crystal I phase; i.e., the structures of the alkyl chains in the crystal I phase are mixed structures of the ordered orthorhombic phase and melted structures corresponding to the columnar phase.
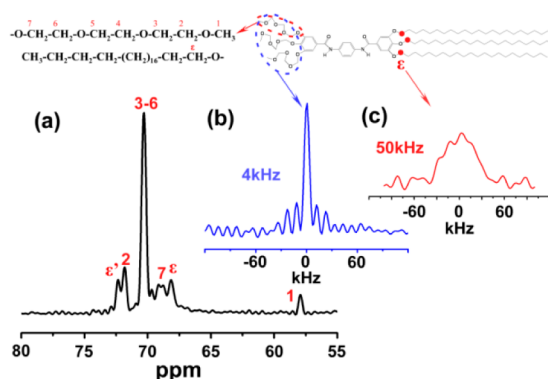

Figure 7. (a) ^{13}C CP/MAS SSNMR spectrum of the TEG tails in the crystal II phase at 363 K and the ^{1}H WISE slice spectra of the inner carbon at (b) 70 ppm (alkyl) and (c) ε-carbons (TEG) at 298 K.

3.4. Molecular Mobility of TEG Tails.
Figure 7a shows the ^{13}C CP/MAS NMR spectrum of the TEG tails and the ^{1}H WISE slice spectra of the inner TEG carbons at 70 ppm, together with those of the ε-carbons in the alkyl chains. The broad ^{1}H line width of 50 kHz for the ε-carbons confirms the restricted dynamics of the alkyl chains at the ε-carbon. However, the narrowed ^{1}H line width of approximately 4 kHz indicates the presence of very fast and large-amplitude molecular motion in the TEG chains at ambient temperature,

corresponding to a melted state. The ^{1}H spectra of the TEG region in the crystal I phase also showed the same results (data not shown here). We concluded that the TEG chains' very high mobility contributed little to the phase transition of these Janus bisamide supramolecules.

3.5. ^{13}C CP/MAS SS NMR Spectra of the Central Aromatic Core.
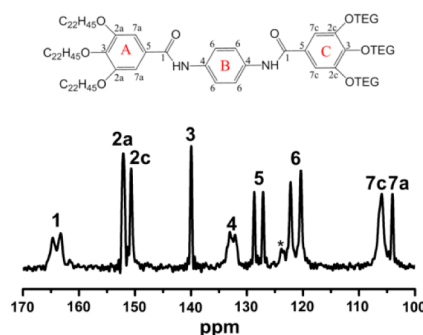Figure 8 shows the ^{13}C CP/MAS NMR

Figure 8. ^{13}C CP/MAS NMR spectrum of the aromatic region in the crystal II phase at 363 K. The * symbol represents the spinning sidebands. The molecular structure and signal assignments are shown.

spectrum of the aromatic region in the crystal II phase at 363 K. Individual signals in three different aromatic rings were clearly separated from each other at high temperatures. The peak assignments were made on the basis of the former solution-state NMR.[8] As the temperature was increased from 233 to 363 K, two characteristic line-shape changes emerged. One change was motional broadening and narrowing of the C6 signals, and maximum line broadening was observed at approximately 293 K. Another change was the coalescence of two signals for C2c signals into one at 343 K. These observations suggest that the A, B, and C rings possess substantially different motilities in the aromatic core constructed via intermolecular hydrogen bonding between N—H and C=O.

Figure 9a shows the temperature dependence of the C6 signals' ^{13}C line width. The temperature dependence of the ^{13}C line width was fitted using eq 5, and the best-fit curve is shown as a solid line in Figure 9a. On the basis of the fitting result, an activation energy E_a of 52 ± 1 kJ/mol and a $\langle \tau_0 \rangle = (8.7 \pm 0.4) \times 10^{-15}$ s were obtained. These two parameters provided $\langle \tau_c \rangle$ values at various temperatures (red circles) using a simple Arrhenius function (Figure 9c). The C2c carbons gave two separate signals at 313 K, which are attributed to two magnetically nonequivalent sites. These two signals merged into one resonance with increasing temperature. The observed line shape change, $I(\omega)$, is described as a function of two site exchange rates, k, using the following equation[20]

$$I(\omega) = \frac{1}{2}$$

$$\frac{k(\omega_1 - \omega_2)^2}{[(\omega - \omega_1)(\omega - \omega_2)]^2 + k^2[2\omega - (\omega_1 + \omega_2)]^2} \quad (11)$$

where ω_1 and ω_2 are the resonance frequency of each site in a rigid limit. Figure 9b shows experimental and calculated line shapes created by adopting Lorentzian peaks with a chemical-shift separation of 90 Hz and a line broadening of 40 Hz. A comparison of the calculated line shape with the experimental shape provided the exchange rate k ($\langle \tau_c \rangle = k^{-1}$) over a wide
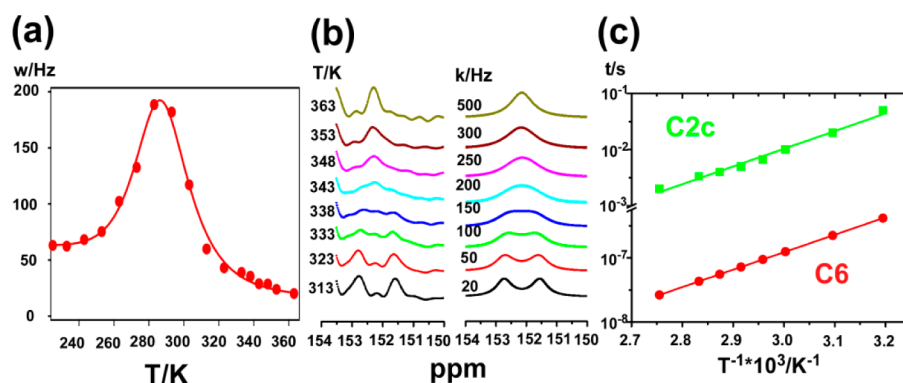
Figure 9. (a) Temperature dependence of the C6 carbon's ^{13}C line width in the aromatic B ring in the crystal II phase, together with the best-fit curve created using eq 6; (b) experimental and calculated temperature dependence of the C2 carbon's ^{13}C line shapes assuming two-site jumps with a chemical shift separation of 90 Hz and Lorentzian broadening of 40 Hz; and (c) correlation time of aromatic rings B (red filled circles) and C (green circles) as functions of temperature.

temperature range. For example, $\langle \tau_c \rangle$ was 0.05 s at 313 K and decreased to 0.002 s at 363 K. The temperature dependence of $\langle \tau_c \rangle$ in the aromatic C ring is plotted in Figure 9c and shows Arrhenius behavior with a best-fit E_a value of 60.6 ± 2.5 kJ/mol. The obtained activation energy is slightly higher than that of the central aromatic ring B, which displayed a frequency 3−4 orders of magnitude greater than that of C at the same temperature.

3.6. Geometry of Molecular Motions of the Aromatic Rings. In addition to understanding the kinetic heterogeneity within the central aromatic core, we also needed to understand the dynamic geometry of all three aromatic rings. Figure 10a
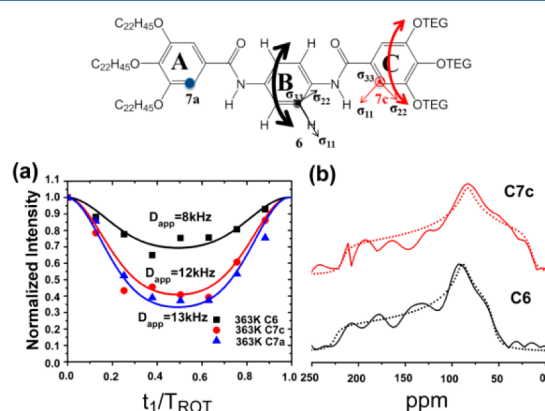

Figure 10. (a) DIPSHIFT dephasing curves of the protonated carbon in the three different phenyl rings at 363 K. The best-fit results are shown as solid lines. (b) ^{13}C experimental (solid curve) and simulated (dotted curve) CSA for C6 (black) and C7c (red) in the crystal II phase at 363 K.

shows the ^{1}H−^{13}C DIPSHIFT dephasing curves of the protonated aromatic carbons in the A (filled blue triangles), B (squares), and C (red circles) rings. C7a displayed the most dephased curve, whereas C6 displayed the least dephased one.

The best-fit simulation results for the individual curves based on eqs 4 and 5 are represented by solid lines in Figure 10a. The rigid limit value for the ^{13}C−^{1}H dipolar coupling strength, assuming an internucleus distance of 1.1 Å, was 22.8 kHz.[47] Under FSLG decoupling, the apparent dipolar coupling strength in a rigid limit was calculated to be 13 kHz using a scaling factor of 0.577 for the FSLG sequence. The experimental DIPSHIFT curve for the C6 carbon was fit with

a calculated curve with an apparent D_{zz} of 8 kHz. According to eq 2, the analytical solution of the ^{13}C−^{1}H dipolar tensor under π-flip motion was calculated to be 8.2 kHz, which is very similar to our experimental result.[27]

The dipolar coupling strengths for aromatic rings A (C7a, D_{zz} = 13 kHz) and C (C7c, 12 kHz) were obtained, as shown in Figure 10a. These results verified the results obtained from the ^{13}C line-width analysis for the C2 carbons in aromatic rings A and C and illustrated the dynamic heterogeneity of the three central aromatic rings.

CSA was also used for further validation of geometry of molecular motions for the aromatic rings. Very small high-resolution NMR signals for the aromatic rings give low signal-to-noise ratios for the corresponding recoupled CSAs. Figure 10b shows the ^{13}C CSA spectra of C7c and C6 at 363 K. The CSA pattern of the C7c carbon ((σ_{11}, σ_{22}, σ_{33}) = (216, 83, 15 ppm)) was much wider than that of the C6 carbon ((σ_{11}, σ_{22}, σ_{33}) = (227, 92, 72 ppm)).

According to the literature, the protonated aromatic rings in the various systems commonly adopt the following CSA principle axis orientations:[27] σ_{11} is parallel to the C−H vector, σ_{22} is normal to the C−H direction, and σ_{33} is perpendicular to the phenyl ring plane. Assuming the same CSA values for C6 in the static case as those of polycarbonate (PC) in a rigid limit, the CSA spectra of the protonated aromatic C6 rings were calculated under different amplitudes of motion for φ = 0, 90, and 180° in a fast motional limit (Figure S2 in the Supporting Information). The aromatic CSA had a large δ value of ca. 111.3 ppm. Therefore, the $\bar{\eta}$ and $\bar{\delta}$ values and corresponding CSA pattern were sensitive to changes in φ (see Figure S3 in the Supporting Information). Only the calculated result with φ = 180° is shown as a dotted curve in Figure 10b and can reproduce the experimental CSA pattern for C6.

The CSA pattern for C7c, calculated on the basis of the experimental principal-axis values, is shown as dotted lines in Figure 10b. The $\bar{\eta}$ value of 0.61 and $\bar{\delta}$ = 111.3 ppm were consistent with the typical static CSA parameters of the protonated aromatic rings, including poly(2-hydroxypropyl ether of bisphenol A) ($\bar{\eta}$ = 0.62 and $\bar{\delta}$ = 113.3 ppm)[48] and PC ($\bar{\eta}$ = 0.64 and $\bar{\delta}$ = 101.7 ppm).[49] This static feature was also consistent with the DIPSHIFT results.

4. DISCUSSION

4.1. Dynamic Nature of the Alkyl Chains' Phase Transitions. The alkyl chain of $C_{22}PhBAEO_3$ in the crystal

II phase performed two-site jumps with a flip angle of 60° in a fast motional limit ($\langle \tau_c \rangle < 10^{-4}$ s) at ambient temperature. Both the dynamic geometry and the $\langle \tau_c \rangle$ were substantially different from those in the *n*-alkanes and PE in the crystalline states. Previous neutron scattering and SSNMR works indicated that *n*-alkanes do not perform dynamically in stable crystalline states.[50,51] Additionally, the $^{13}C-^{13}C$ dipolar exchange NMR showed that PE stems in the crystalline regions performed a 180° flip motion with $\langle \tau_c \rangle = 10^{-1}$ s at ambient temperature.[52] This slow dynamics included overall 180° rotations concomitant with translations of the overall stems by one monomer unit along the stem axis. The collective dynamics of local flips resulted in chain diffusions.

At this point, we comment on the structural origins of the different molecular dynamics of the alkyl chains in $C_{22}PhBAEO_3$ compared to those in *n*-alkanes and PE in the crystalline regions. According to the crystalline structures, the orthorhombic *a* and *b* unit-cell parameters for PE and *n*-alkanes such as $C_{21}H_{46}$ are *a* = 7.40 and *a* = 4.93 Å[53] and *a* = 7.47 and *c* = 4.97 Å),[54] respectively, at ambient temperature, whereas the parameters are *a* = 7.80 and *c* = 4.98 Å for the crystal II phase,[8] where only the *a* value is substantially longer than those of the *n*-alkane and PE. This is a characteristic difference between PE and *n*-alkanes, and the alkyl chains in the crystal II phase of $C_{22}PhBAEO_3$. The longer *a*-value can be explained in terms of the topological constraints of the alkyl chains anchored to the aromatic core. These topological constraints allow for looser packing of the alkyl chains in $C_{22}PhBAEO_3$ compared to those of *n*-alkanes and PE. Such loose packing would be a source of the alkyl chains' very high mobility in the crystal II phase. Another structural difference is the chemical connectivity with the aromatic group. In PE, the stems are connected to the flexible amorphous segments at the interface between the crystal and amorphous regions. Thus, chain diffusions along the *c*-axis lead to conformational changes in the flexible segments in the interfacial and amorphous regions. In the case of the alkyl chains in $C_{22}PhBAEO_3$, the chain end is chemically connected via a flexible oxygen linkage to the rigid aromatic A-ring. The aromatic positions are fixed via intermolecular hydrogen bonding. Thus, only the flexible oxygen linkage can change its conformation due to the rotations and translations of the alkyl chains. However, only one oxygen displacement physically limits the alkyl chains' translation distances. Such constraints along the *c*-axis essentially restrict both translations and rotations of the alkyl chains, which is why the dynamic amplitude of the alkyl chains in $C_{22}PhBAEO_3$ is limited to smaller amplitudes (ca. 60°) than those in PE.

n-Alkanes, PE, and the alkyl chains in $C_{22}PhBAEO_3$ experienced phase transitions from stable crystalline phases into hexagonal (pseudohexagonal) phases. Large differences were observed in both the dynamic geometry and the kinetic parameters of the alkyl chains between *n*-alkanes, PE, and the crystal II phase of $C_{22}PhBAEO_3$ during the phase transitions. In the crystal II phase, the alkyl chains essentially maintained similar geometry of molecular motions (ca. 65°), even after the phase transitions. Topological constraints similarly restricted the dynamic geometry of the alkyl chains in the pseudohexagonal phase. Figure 11a shows the $^{13}C-^1H$ dipolar dephasing curve of the alkyl chains' CH_2 signals in the crystal II phase at various temperatures. The dipolar coupling strength of the alkyl chains' CH_2 groups in the crystal II phase continuously decreased from 12.5 kHz at ambient temperature to 9.5 kHz at 363 K. Such a continuous decrease simply indicates that the
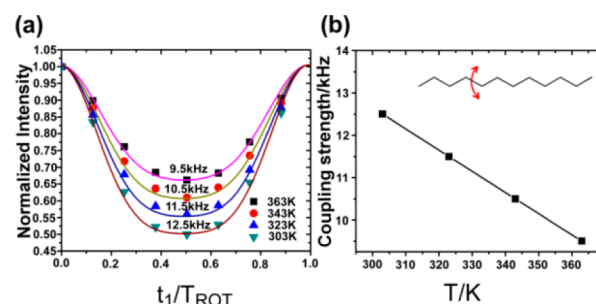

Figure 11. (a) DIPSHIFT dephasing curve of the CH_2 alkyl chains together with the curves calculated from eqs 4 and 5 and (b) corresponding dipolar coupling strengths at various temperatures.

mobility of the alkyl chains is thermally activated across the transition temperatures; i.e., no sudden jump in molecular mobility before and after the transition was observed. Such continuous dynamics differ substantially from that in the *n*-alkanes and PE. For example, *n*-$C_{19}H_{40}$ showed drastic dynamic changes—from no molecular dynamics in the orthorhombic phase at 293 K to rotational diffusions in a fast motional limit at 298 K.[50] At high temperatures and pressures, the ^2H quadrupole line shapes in PE also changed suddenly from a 180° flip motion at 500 K to continuous rotations at 503 K.[38] These discontinuous changes in both dynamic geometry and $\langle \tau_c \rangle$ were origins of the exothermic peaks during the phase transitions. On the basis of these discussions, we concluded that the thermally continuous activation of dynamics and the lack of geometry change in the alkyl chains during the orthorhombic/pseudohexagonal phase transition are responsible for the lack of an exothermic peak in the crystal II phase of $C_{22}PhBAEO_3$. The unique dynamics observed in the alkyl chains were intrinsic dynamics in the supramolecules, where different elements were chemically connected via covalent bonds and unique self-assembly structures were determined through multiple interactions. Such a unique molecular and 3D structure indicated a new structure and, consequently, led to a new thermal property that was substantially different from the thermal properties of the structural elements themselves.

4.2. Relationship between the Aromatic Dynamics and Structures. The NMR results clearly detected the dynamic heterogeneity of the three aromatic rings in the crystal II phase. Only the aromatic B-ring exhibited very fast dynamics ($\langle \tau_c \rangle \sim 10^{-5}$ s at ambient temperature). Usually, within both simple organic molecules and complex supramolecules such as aromatic rings, $\pi-\pi$ interactions are a driving force in the construction of self-assembly structures.[11,12] In the case of this Janus bisamide molecule, intermolecular hydrogen bonding is the dominant interaction instead of $\pi-\pi$ interactions.[8] This hydrogen bonding builds up a unique space for all three aromatic rings, in which the *d*-spacing is 7–10 Å.[8] Thus, the A- and C-rings also have open spaces similar to those in B. Actually, aromatic rings A and C are anchored by three hydrophilic and hydrophobic tails, respectively. Therefore, additional anchored chains and their phase structures significantly influence the two aromatic rings' dynamics, even though the TEG tails show liquidlike dynamics, even at ambient temperature. Three flexible chains allow for slow dynamics with a frequency of 400 Hz at a very high temperature of 363 K. The aromatic A-ring anchored by the alkyl chains that form orthorhombic and pseudohexagonal phases at temperatures greater than 323 K do not perform any

molecular dynamics at the available temperature. The molecular dynamics of the three aromatic rings is significantly affected by the available dynamic spaces formed via intermolecular hydrogen bonds and by the phase structures and mobility of the anchored chains. Topological constraints based on complex chemical architectures and physical spaces constructed by hydrogen-bonding interactions thus determine the molecular dynamics of the three central aromatic rings.

4.3. Phase-Transition Behavior.
In general, molecules that consist of rigid cores and flexible chains have difficulty exhibiting 3D long-range order due to their flexible chains. The asymmetric Janus bisamide supramolecule can form a 3D long-range ordered structure. We have previously described the structural formation process of the crystal II phase as follows. The basic Janus unit is constructed via (i) an orthogonal hydrogen bond between N−H and C=O, (ii) microphase separation due to repulsion of the rigid aromatic core and flexible side chains, and (iii) hydrophilic/hydrophobic interactions, as illustrated in Figure 1a−c. The key issue with regard to the 3D long-range order in asymmetric Janus bisamide supramolecules is the formation of long-range order in the alkyl chains. As previously demonstrated, the TEG chains in the crystal II phase are highly disordered states that do not contribute to the long-range order. However, hydrophobic/hydrophilic repulsion induces separation of the alkyl chains from the TEG chains and consequently limits the available spaces for crystallization of the alkyl chains. Thus, the TEG chains also play a very important role in the 3D long-range order of asymmetric Janus bisamide supramolecules.

On the basis of viewpoints of molecular structure and dynamics, we comment on the formation route (columnar phase → crystal II phase) of the 3D long-range order of the Janus supramolecular system $C_{22}PhBAEO_3$. The cooling process from the columnar phase induced a metastable crystal I phase. High-resolution NMR detected *trans*- and *gauche*-rich conformations for the alkyl chains. In addition, recoupled CSA patterns for the inner and end parts clearly indicated that the alkyl chain structures in the crystal I phase are locally mixed structures of the crystal II phase and the melted state (columnar phase). The difference between the crystal I and II phase is the length scale and fraction of the ordered regions. The rapid crystallization process does not allow the alkyl chains to adopt 3D long-range order in the crystal I phase. Thus, the kinetically driven crystallization of the alkyl chains induces slightly different local orientations from one domain to another. The fixed orientations of the alkyl chains in individual domains also fix the orientations of the aromatic A-ring. Thus, the slightly different orientations of the aromatic core domains do not allow for the complete crystallization of all alkyl chains in the solid phase. For this reason, the complete melting of the alkyl chains in the crystal I phase is necessary to induce 3D long-range order in the alkyl chains. The disordered fraction of the alkyl chains was determined to be 14% at ambient temperature, which would have originated from the interfacial regions between two locally ordered domains. The disordered regions increased continuously with increasing temperature and finally melted completely at temperatures above 353 K. After the melting of the short-range-ordered alkyl chains, local orientations of the aromatic rings disappeared. Only slow crystallization of the alkyl chains from the melted state provided 3D long-range order in either the alkyl chains or the aromatic cores, which is the reason why annealing of the crystal I phase did not induce the formation of the stable crystal II phase and

why the columnar phase, or complete melting of the crystal I phase, was necessary for the formation of the stable crystal II phase.

5. CONCLUSION
The molecular dynamics of the alkyl and TEG chains and all three rigid aromatic rings of Janus bisamide $C_{22}PhBAEO_3$ were thoroughly studied by SSNMR spectroscopy. The alkyl chains in the stable crystal II phase performed unique two-site jumps with a jump angle of ca. 60° in the orthorhombic phase. The alkyl chains also maintained the same geometry at high temperatures, even across the orthorhombic pseudohexagonal transition temperature. Continuously activated molecular dynamics across the transition temperature reasonably explained the lack of an exothermic peak in the DSC thermogram. In addition, site-selective CSA ensured that the α-carbon in the alkyl chain close to the chain end also exhibited the same geometry as the inner alkyl chains in the orthorhombic and pseudohexagonal phases; i.e., the molecular dynamics of the alkyl chain were spatially homogeneous in the crystal II phase, possessing 3D long-range order. In the crystal I phase, high-resolution NMR gave a *trans* conformation fraction of 86% at ambient temperature. The *trans* conformation exhibited the same dynamic geometry as the alkyl chains in the crystal II phase, whereas the *gauche*-rich conformation exhibited near-isotropic motion. In addition, the α-carbon had two components of uniaxial jump motion and near-isotropic motion. This observation clearly indicated that the alkyl chains in the crystal I phase possessed two local phase structures of the crystal II and columnar phases. The structural heterogeneity, once formed by kinetics, could not allow the alkyl chains to construct complete 3D long-range order in the solid phase because the crystalline domain of the alkyl chains did not allow the aromatic rings to be properly rearranged in the solid phase due to different chemical connections. The construction of 3D long-range order in the entire molecule therefore required the complete destruction of the alkyl chain structures' local orders in the crystal I phase. The TEG chains exhibited very fast liquidlike motions at ambient temperature in both the crystal I and II phases. These dynamics did not contribute to phase transitions at high temperatures. However, hydrophobic/hydrophilic repulsions limited the available spaces for crystallizable alkyl chains and indirectly supported the formation of 3D long-range order. Therefore, unique asymmetric flexible tails were very important factors in the construction of self-assembly structures with 3D long-range order. The dynamics of the central aromatic core clearly supported the structural formation process via hydrogen-bonding interactions proposed by Cheng et al.[8] Only the central B-ring performed 180° flip motions in a fast motional limit. These unique and fast dynamics were produced via open spaces constructed by the hydrogen bonding of C=O and N−H in two molecules orthogonal to each other. Such fast dynamics was largely different from the dynamics in sheet structures formed via the $\pi-\pi$ interactions of a traditional columnar structure. In addition, the other A and C aromatic rings, which possessed dynamic spaces similar to those of the B-ring, were chemically linked to three alkyl and TEG chains, respectively, giving slow dynamics or no dynamics at temperatures up to 363 K. These unique aromatic dynamics were reasonably explained by the mobility of anchored alkyl and TEG chains and their phase structures. These molecular dynamic analyses, performed by SS-NMR at the atomic level,

significantly contributed to our understanding of the structural formation and transition mechanisms of complex self-assembly systems in supramolecular chemistry.[6]

■ ASSOCIATED CONTENT

S Supporting Information

Dynamic models and calculated asymmetry and anisotropy parameters for the CSA of alkyl chains and aromatic rings. This material is available free of charge via the Internet at http://pubs.acs.org.

■ AUTHOR INFORMATION

Corresponding Author

*E-mail: miyoshi@uakron.edu. Tel.: 1-330-972-6269.

Notes

The authors declare no competing financial interest.

■ ACKNOWLEDGMENTS

■ REFERENCES

(1) Ariga, K.; Kunitake, T. *Supramolecular chemistry: fundamentals and applications: advanced textbook*; Springer: New York, 2006.

(2) Lehn, J. M. *Supramolecular Chemistry*; Wiley-VCH: Weinheim, Germany, 1995.

(3) Lehn, J. M. Supramolecular Chemistry—Scope and Perspectives Molecules, Supermolecules, and Molecular devices (Nobel Lecture). *Angew. Chem., Int. Ed. Engl.* **1988**, *27*, 89−112.

(4) De Gennes, P. G. Pincements de Skoulios et structures incommensurables. *J. Phys. (Paris), Lett.* **1983**, *44*, 657−664.

(5) Anderson, P. W. Absence of Diffusion in Certain Random Lattices. *Phys. Rev.* **1958**, *109*, 1492−1505.

(6) Spiess, H. W. Interplay of Structure and Dynamics in Macromolecular and Supramolecular Systems. *Macromolecules* **2010**, *43*, 5479−5491.

(7) Ober, C. K.; Cheng, S. Z. D.; Hammond, P. T.; Muthukumar, M.; Reichmanis, E.; Wooley, K. L.; Lodge, T. P. Research in Macromolecular Science: Challenges and Opportunities for the Next Decade. *Macromolecules* **2009**, *42*, 465−471.

(8) Sun, H. J.; Wang, C. L.; Hsieh, I.-F.; Hsu, C. H.; Van Horn, R. M.; Tsai, C. C.; Jeong, K. U.; Lotz, B.; Cheng, S. Z. D. Phase Behaviour and Janus Hierarchical Supramolecular Structures Based on Asymmetric Tapered Bisamide. *Soft Matter* **2012**, *8*, 4767−4779.

(9) Lee, M.; Kim, J. W.; Peleshanko, S.; Larson, K.; Yoo, Y. S.; Vaknin, D.; Markutsya, S.; Tsukruk, V. V. Amphiphilic Hairy Disks with Branched Hydrophilic Tails and a Hexa-*peri*-hexabenzocoronene Core. *J. Am. Chem. Soc.* **2002**, *124*, 9121−9128.

(10) Hansen, M. R.; Feng, X.; Macho, V.; Müllen, K.; Spiess, H. W.; Floudas, G. Fast and Slow Dynamics in a Discotic Liquid Crystal with Regions of Columnar Order and Disorder. *Phys. Rev. Lett.* **2011**, *107*, 257801.

(11) Elmahdy, M. M.; Floudas, G.; Mondeshki, M.; Spiess, H. W.; Dou, X.; Müllen, K. Origin of the Complex Molecular Dynamics in Functional Discotic Liquid Crystals. *Phys. Rev. Lett.* **2008**, *100*, 107801.

(12) Leisen, J.; Werth, M.; Boeffel, C.; Spiess, H. W. Molecular Dynamics at the Glass Transition: One Dimensional and Two Dimensional Nuclear Magnetic Resonance Studies of a Glass Forming Discotic Liquid Crystal. *J. Chem. Phys.* **1992**, *97*, 3749−3759.

(13) Ungar, G. Structure of Rotator Phases in n-Alkanes. *J. Phys. Chem.* **1983**, *87*, 689−695.

(14) Ungar, G. From Plastic-crystal Paraffins to Liquid-crystal Polyethylene: Continuity of the Mesophase in Hydrocarbons. *Macromolecules* **1986**, *19*, 1317−1324.

(15) Ungar, G.; Masic, N. Order in the Rotator Phase of n-Alkanes. *J. Phys. Chem.* **1985**, *89*, 1036−1042.

(16) Sirota, E. B.; King, H. E., Jr.; Singer, D. M.; Shao, H. H. Rotator phases of the normal alkanes: An x-ray scattering study. *J. Chem. Phys.* **1993**, *98*, 5809−5824.

(17) Bielecki, A.; Burum, D. P. Temperature Dependence of ^{207}Pb MAS Spectra of Solid Lead Nitrate. An Accurate, Sensitive Thermometer for Variable-Temperature MAS. *J. Magn. Reson. A.* **1995**, *116*, 215−220.

(18) Schmidt-Rohr, K.; Clauss, J.; Spiess, H. W. Correlation of Structure, Mobility, and Morphological Information in Heterogeneous Polymer Materials by two-dimensional WIdeline-SEparation NMR spectroscopy. *Macromolecules* **1992**, *25*, 3273−3277.

(19) Dixon, W. T.; Schaefer, J.; Sefcik, M. D.; Stejskal, E. O.; McKay, R. A. Total suppression of sidebands in CPMAS C-13 NMR. *J. Magn. Reson.* **1982**, *49*, 341−345.

(20) Mehring, M. *High-Resolution NMR in Solids*; Springer-Verlag: Berlin, 1983.

(21) Liu, S.-F.; Mao, J.-D.; Schmidt−Rohr, K. A Robust Technique for Two-Dimensional Separation of Undistorted Chemical-Shift Anisotropy Powder Patterns in Magic-Angle-Spinning NMR. *J. Magn. Reson.* **2002**, *155*, 15−28.

(22) Hong, M.; Gross, J. D.; Rienstra, C. M.; Griffin, R. G.; Kumashiro, K. K.; Schmidt−Rohr, K. Coupling Amplification in 2D MAS NMR and Its Application to Torsion Angle Determination in Peptides. *J. Magn. Reson.* **1997**, *129*, 85−92.

(23) Hackel, C.; Zinkevich, T.; Belton, P.; Achilles, A.; Reichert, D.; Krushelnitsky, A. The Trehalose Coating Effect on the Internal Protein Dynamics. *Phys. Chem. Chem. Phys.* **2012**, *14*, 2727−2734.

(24) Cobo, M. F.; Achilles, A.; Reichert, D.; deAzevedo, E. R.; Saalwachter, K. Recoupled Separated-local-field Experiments and Applications to Study Intermediate-regime Molecular Motions. *J. Magn. Reson.* **2012**, *221*, 85−96.

(25) Munowitz, M. G.; Griffin, R. G.; Bodenhausen, G.; Huang, T. H. Two-Dimensional Rotational Spin-Echo Nuclear Magnetic Resonance in Solids: Correlation of Chemical Shift and Dipolar Interactions. *J. Am. Chem. Soc.* **1981**, *103*, 2529−2533.

(26) Bielecki, A.; Kolbert, A.; Levitt, M. Frequency-Switched Pulse Sequences: Homonuclear Decoupling and Dilute Spin NMR in Solids. *Chem. Phys. Lett.* **1989**, *155*, 341−346.

(27) Schmidt−Rohr, K.; Spiess, H. W. *Multidimensional Solid−State NMR and Polymers*; Academic Press: London, 1994.

(28) Miyoshi, T.; Mamun, A.; Reichert, D. Fast Dynamics and Conformations of Polymer in a Conformational Disordered Crystal Characterized by $^{1}H−$ ^{13}C WISE NMR. *Macromolecules* **2010**, *43*, 3986−3989.

(29) Takegoshi, K.; Hikichi, K. Effects of Blending on Local Chain Dynamics and Glass Transition: Polystyrene/Poly(vinyl methyl ether) Blends as Studied by High-Resolution Solid-state ^{13}C Nuclear Magnetic Resonance Spectroscopy. *J. Chem. Phys.* **1991**, *94*, 3200−3206.

(30) Kaji, H.; Tai, T.; Horii, F. One-and Two-Dimensional MAS ^{13}C NMR Analyses of Molecular Motions in Poly (2-hydroxypropyl Ether of Bisphenol-A). *Macromolecules* **2001**, *34*, 6318−6324.

(31) VanderHart, D. L.; Earl, W. L.; Garroway, A. N. Resolution in Carbon-13 NMR of Organic Solids Using High-Power Proton Decoupling and Magic-Angle Sample Spinning. *J. Magn. Reson.* **1981**, *44*, 361−401.

(32) Rothwell, W. P.; Waugh, J. S. Transverse Relaxation of Dipolar Coupled Spin Systems Under rf Irradiation: Detecting Motions in Solids. *J. Chem. Phys.* **1981**, *74*, 2721−2732.

(33) Clauss, J.; Schmidt-Rohr, K.; Adam, A.; Boeffel, C.; Spiess, H. W. Stiff Macromolecules with Aliphatic Side Chains: Side-Chain Mobility, Conformation, and Organization from 2D Solid-State NMR Spectroscopy. *Macromolecules* **1992**, *25*, 5208−5214.

(34) Kitamaru, R.; Horii, F.; Nakagawa, M.; Takamizawa, K.; Urabe, Y.; Ogawa, Y. Solid-Solid Phase Transformation of Uniaxially Oriented n-Alkane Crystals of High Purity. *J. Mol. Struct.* **1995**, *355*, 95−104.

13708

dx.doi.org/10.1021/jp4081492 | *J. Phys. Chem. B* 2013, 117, 13698−13709

(35) Ishikawa, S.; Kurosu, H.; Ando, I. Structural Studies of n-Alkanes by Variable-Temperature Solid-State High-Resolution ^{13}C NMR Spectroscopy. *J. Mol. Struct.* **1991**, *248*, 361−372.

(36) Kuwabara, K.; Horii, F. Solid-State ^{13}C NMR Analyses of the Orthorhombic-to-Hexagonal Phase Transition for Constrained Ultra-drawn Polyethylene Fibers. *Macromolecules* **1999**, *32*, 5600−5605.

(37) Bassett, D. C.; Khalifa, B. A.; Turner, B. Chain-Extended Crystallization of Polyethylene. *Nature (Phys. Sci.)* **1972**, *239*, 106−108.

(38) De Langen, M.; Prins, K. O. Mobility of Polyethylene Chains in the Orthorhombic and Hexagonal Phases Investigated by NMR. *Chem. Phys. Lett.* **1999**, *299*, 195−200.

(39) VanderHart, D. L. Influence of Molecular Packing on Solid-State ^{13}C Chemical Shifts: The *n*-Alkanes. *J. Magn. Reson.* **1981**, *44*, 117−125.

(40) Muller, A. An X-Ray Investigation of Normal Paraffins Near Their Melting Points. *Proc. R. Soc. London A* **1932**, *138*, 514−530.

(41) Barnes, J. D.; Fanconi, B. M. Raman Spectroscopy, Rotational Isomerism, and the "Rotator" Phase Transition in n-Alkanes. *J. Chem. Phys.* **1972**, *56*, 5190−5192.

(42) Nakagawa, M.; Horii, F.; Kitamaru, R. Phase Structure of Uniaxially Oriented Polyethylene Films as Studied by High Resolution Solid State ^{13}C N.M.R. Spectroscopy. *Polymer* **1990**, *31*, 323−328.

(43) Möller, M.; Gronski, W.; Cantow, H.-J.; Höcker, H. Discrimination of Rotational Isomeric States in Cycloalkanes by Solid-State CP-MAS carbon-13 NMR Spectroscopy. *J. Am. Chem. Soc.* **1984**, *106*, 5093−5099.

(44) Möller, M.; Cantow, H.-J.; Drotloff, H.; Emeis, D.; Lee, K. S.; Wegner, G. Phase Transitions and Defect Structure in the Lamellar Surface of Polyethylene and n-Alkane Crystallites. Magic Angle Spinning ^{13}C NMR Studies. *Macromol. Chem.* **1986**, *187*, 1237−1252.

(45) Shen, H.; Jeong, K.-U.; Xiong, H.; Graham, M. J.; Leng, S.; Zheng, J. X.; Huang, H.; Guo, M.; Harris, F. W.; Cheng, S. Z. D. Phase Behaviors and Supra-molecular Structures of a Series of Symmetrically Tapered Bisamides. *Soft Matter* **2006**, *2*, 232−242.

(46) Xue, C.; Jin, S.; Weng, X.; Ge, J. J.; Shen, Z.; Shen, H.; Graham, M. J.; Jeong, K.-U.; Huang, H.; Zhang, D.; et al. Self-assembled "Supra-molecular" Structures via Hydrogen Bonding and Aromatic/Aliphatic Microphase Separation on Different Length Scales in Symmetric-Tapered Bisamides. *Chem. Mater.* **2004**, *16*, 1014−1025.

(47) Reichert, D.; Pascui, O.; Deazevedo, E. R.; Bonagamba, T. J.; Arnold, K.; Huster, D. A Solid-State NMR Study of the Fast and Slow Dynamics of Collagen Fibrils at Varying Hydration Levels. *Magn. Reson. Chem.* **2004**, *42*, 276−284.

(48) Kaji, H.; Fuke, K.; Horii, F. Two-Dimensional ^{13}C Magic Angle Turning NMR Analyses of Dynamics in Poly (2-hydroxypropyl ether of bisphenol A). *Macromolecules* **2003**, *36*, 4414−4423.

(49) Graf, R.; Ewen, B.; Spiess, H. W. Geometry of Phenylene Motion in Polycarbonate from NMR Spectroscopy and Neutron Scattering. *J. Chem. Phys.* **2007**, *126*, 041104.

(50) Taylor, M. G.; Kelusky, E. C.; Smith, I. C.; Casal, H. L.; Cameron, D. G. A ^{2}H NMR Study of the Solid-Phase Behavior of Nonadecane. *J. Chem. Phys.* **1983**, *78*, 5108−5112.

(51) Guillaume, F.; Doucet, J.; Sourisseau, C.; Dianoux, A. J. Molecular Motions in n-Nonadecane $C_{19}H_{40}$: An Incoherent Neutron Scattering Study. *J. Chem. Phys.* **1989**, *91*, 2555−2567.

(52) Hu, W. G.; Boeffel, C.; Schmidt-Rohr, K. Chain Flips in Polyethylene Crystallites and Fibers Characterized by Dipolar ^{13}C NMR. *Macromolecules* **1999**, *32*, 1611−1619.

(53) Bassett, D. C.; Block, S.; Piermarini, G. J. A High Pressure Phase of Polyethylene and Chain Extended Growth. *J. Appl. Phys.* **1974**, *45*, 4146−4150.

(54) Craig, S. R.; Hastie, G. P.; Roberts, K. J.; Shenvood, J. N. Investigation Into the Structures of some Normal Alkanes within the Homologous Series $C_{13}H_{28}$ to $C_{60}H_{122}$ Using High-Resolution Synchrotron X-ray Powder Diffraction. *J. Mater. Chem.* **1994**, *4*, 977−981.